

Relevance of Cu-3d multiplet structure in models of high T_c cuprates

Mi Jiang, Mirko Moeller, Mona Berciu, and George A. Sawatzky

*Department of Physics and Astronomy, University of British Columbia, Vancouver B.C. V6T 1Z1, Canada and
Stewart Blusson Quantum Matter Institute, University of British Columbia, Vancouver B.C. V6T 1Z4, Canada*

We revisit the problem of the spectra of two holes in a CuO_2 layer, modeled as a Cu-d^8 impurity with full multiplet structure coupled to a full O-2p band as an approximation to the local electronic structure of a hole doped cuprate. Unlike previous studies that treated the O band as a featureless bath, we describe it with a realistic tight binding model. While our results are in qualitative agreement with previous work, we find considerable quantitative changes when using the proper O-2p band structure. We also find (i) that only the ligand O-2p orbitals play an essential role, within this impurity model; (ii) that the three-orbital Emery model provides an accurate description for the subspace with 1A_1 symmetry, which includes the ground-state in the relevant region of the phase diagram; (iii) that this ground-state has only $\sim 50\%$ overlap with a Zhang-Rice singlet; (iv) that there are other low-energy states, in subspaces with different symmetries, that are absent from the three-orbital Emery model and its one-band descendants. These states play an important role in describing the elementary excitations of doped cuprates.

I. INTRODUCTION

A central issue still under debate in the study of high- T_c cuprate superconductors is the proper minimal model that correctly captures the low-energy properties, specifically the precise nature of the states closest to the Fermi level. Historically, Anderson proposed that the essential physics can be understood based on the single-band Hubbard model, where the band is identified as the antibonding band of $\text{Cu-}3d_{x^2-y^2}$ and O-2p orbitals.¹ The even simpler t-J model additionally discards all doubly occupied states and describes a square lattice where charge carriers move in a spin background. This has been extensively studied away from half-filling and is believed to provide a good description of the Hubbard model in the strong coupling limit $J/t = 4t/U \ll 1$. However, their common intrinsic assumption is that the cuprate parents compounds, which are known to be charge transfer insulators², can instead be modeled as effective Mott-Hubbard insulators.

The need to understand the importance of explicitly including the O ions hosting the doped holes, motivated the study of the three-band Emery model³, which includes the Cu $d_{x^2-y^2}$ and the two ligand O-2p $_{\sigma}$ orbitals in the non-magnetic unit cell. The key idea underlying the expected equivalence of the one- and three-orbital scenarios was proposed by Zhang and Rice, who argued that the doped holes occupy a certain linear combination of O orbitals that is locked into a Zhang-Rice singlet (ZRS) with the hole (spin) residing on the central Cu site. Projecting onto these ZRS then allows one to map the three-band Emery model onto a single-band t-J model,⁴ although a more careful treatment reveals the existence of additional terms ignored by the t-J Hamiltonian.^{5,6}

Although various analytical approximations and extensive numerical studies of these model Hamiltonians have revealed many insights in the past decades, the validity of the ZRS concept^{7,8} and more generally the equivalence – or lack thereof – between the low-energy properties of one- and three-orbital models are still under

debate. On one hand, the existence and stability of states with ZRS-like character have been confirmed in previous photoemission experiments.^{9–11} On the other hand, recent calculations contrasting the dynamics of a single doped hole in the one-band *vs.* the three-band model revealed qualitative differences,^{12,16,17} such as the essential *vs.* the minor role played by the background spin-fluctuations, respectively. Moreover, a recent high-energy optical conductivity study questioned the ZRS argument by revealing a strong mixture of singlet and triplet configurations in the lightly hole-doped Zn-LSCO single crystal.⁷ Furthermore, this system exhibits strong ferromagnetic correlations between Cu spins near the doped holes, as predicted by the three-band model.¹²

During the same period when the ZRS was proposed, Eskes *et al.* carried out a more general study that included the multiplet structure of the Cu, *i.e.* all singlet and triplet irreducible representations in the D_{4h} point group spanned by two d holes (d^8 -type configurations) and their corresponding Coulomb and exchange interactions^{13–15}, besides explicitly considering the O band. This was achieved at the cost of simplifying the model to consist of a single Cu impurity hybridizing with a broad O band described in terms of a featureless, semielliptical density of states.

This work confirmed that the first ionization state starting from a Cu- d^9 state and a full O-2p band, which ends with the two hole eigenstates involving d^8 multiplets and various continuum states, is indeed in the 1A_1 symmetry channel consistent with the symmetry of the ZRS, but also found that the energy difference between the lowest ionization states for various symmetry channels is rather small. Moreover, these differences are strongly dependent on the electronic structure, which in turn is likely to depend quite strongly on doping levels. These results cast doubt on whether it suffices to include only the $d_{x^2-y^2}$ orbital instead of the full 3d multiplet structure of the Cu- d^8 , when modeling these materials.

Most members of our community believe that the Cu- $d_{x^2-y^2}$ orbital is the only d-orbital needed to account for

the essential physics of cuprates, explaining why there are so few studies on the effects of the multiplet structure, compared to the very extensive investigations of the one- and three-band models involving only Cu $d_{x^2-y^2}$ orbital and/or its ZRS daughter. However, there are both theoretical and experimental results pointing out the importance of non-planar orbitals like Cu- $3d_{3z^2-r^2}$ and/or O- $2p_z$ ¹⁹⁻³⁰. In particular, the importance of Cu- $3d_{3z^2-r^2}$ is revealed by the recent discovery³⁰ of the cuprate superconductor $\text{Ba}_2\text{CuO}_{4-\delta}$ with critical temperature $T_c \sim 70$ K, where based on the compressed c-axis bond length, it is claimed that some doped holes are likely in the $d_{3z^2-r^2}$ orbital. Early Auger spectroscopic experiments³¹ clearly demonstrated strong multiplet effects ranging over a large energy scale in Cu compounds such as CuO and Cu_2O . In fact, in Cu_2O the lowest energy Cu d^8 state is a triplet state consistent with the Hund's rule expectations. As pointed out by Eskes^{13,14}, the crossing of the singlet and triplet states in the cuprate parent compounds is a result of the strong O character in these states due to the strong Cu-O hybridization and the fact that the Cu d^8 states are pushed out of the top of the O 2p band resulting in the lowest energy singlet bound states^{9,10,31}.

Also important evidence for the significant role of the multiplets comes from X-ray absorption (XAS) experiments that have shown, upon increased doping, a strong change from purely x, y polarized absorption to one including a large contribution of z polarized intensity for the O and Cu core-to-valence transition¹⁹. This implies that there are doped holes whose wavefunctions have a considerable component in the Cu- $d_{3z^2-r^2}$ or O- p_z orbitals. These results point to the breakdown of the single-band or even three-band (Cu- $d_{x^2-y^2}$ based) approaches to the description of the phase diagram of cuprate superconductors.

This motivates us to revisit the importance of the full Cu-3d multiplet structure and explore its effects on the low-energy properties of cuprate models. In order to obtain numerically exact results, we follow Eskes *et al.* and study a single Cu impurity with all its 3d orbitals included. In contrast to this earlier work, however, we properly embed this Cu impurity in a square lattice of O 2p orbitals, with a realistic band-structure. This allows us to contrast models containing only the O-2p ligand orbitals *vs.* those also including the other in-plane orbital, and also the p_z orbital. The results reveal the importance of the realistic modeling of the O bath, and which O-2p orbitals play an essential role. It is important to note that the linear combination of O 2p orbitals that hybridize with the various Cu 3d states live in different energy regions of the O 2p band structure and this strongly influences the importance of this hybridization. For example, the d_{xz} orbital hybridizes with the O- p_z and p_x π -bonding orbitals while the $d_{x^2-y^2}$ orbital hybridizes with the O-2p σ -bonding orbitals. Besides, the linear combination of the O-2p orbitals that hybridize with $d_{x^2-y^2}$ orbital is different in

their relative phases than with the $d_{3z^2-r^2}$ orbital. We will see below how this strongly influences the appearance and relative energies of bound states pushed out of the O band for the various symmetries. Furthermore, by calculating the Cu-3d electron removal spectra in various symmetry channels of the D_{4h} point group, we are able to identify the character (symmetry, spin, and orbital composition) of the first ionization state, and to gauge its similarity to a ZRS. Finally, our results reveal strong similarities between the model including all multiplets and the conventional three-orbital Emery model if we restrict ourselves to the lowest energy electron removal states, although open issues still remain. However, if one wants to describe the spectroscopies like ARPES going up to one or more eV below the Fermi energy as, for example, in descriptions of the so called “waterfall” feature³², it is essential to include all of the multiplets since they all have appreciable spectral weights extending to energies well above 1 eV.

This paper is organized as follows. In Sec. II, we define our model and the variational method employed to study its single-doped hole eigenstates. Sec. III discusses the resulting spectra for various cases considered. The summary and future issues to be addressed are presented in Sec. IV.

II. MODELS AND METHODS

A. Multi-orbital models with a single Cu impurity

We simplify the description of a CuO_2 plane by replacing the Cu lattice with a single Cu impurity properly embedded in a square lattice of O orbitals; the resulting problem can be solved exactly, unlike the corresponding one for the full CuO_2 lattice. The central part of the system, consisting of the Cu impurity and its 4 nearest neighbor (NN) O ions, is depicted in Fig. 1. The Hamiltonian describing this system is

$$\begin{aligned}
 H &= E_s + K_{pd} + K_{pp} + V_{dd} + V_{pp} \\
 E_s &= \sum_{m\sigma} \epsilon_d(m) d_{m\sigma}^\dagger d_{m\sigma} + \sum_{jn\sigma} \epsilon_p p_{jn\sigma}^\dagger p_{jn\sigma} \\
 K_{pd} &= \sum_{\langle j \rangle mn\sigma} (T_{mn}^{pd} d_{m\sigma}^\dagger p_{jn\sigma} + h.c.) \\
 K_{pp} &= \sum_{\langle jj' \rangle nn'\sigma} (T_{nn'}^{pp} p_{jn\sigma}^\dagger p_{j'n'\sigma} + h.c.) \\
 V_{dd} &= \sum_{\bar{m}_1 \bar{m}_2 \bar{m}_3 \bar{m}_4} U(\bar{m}_1 \bar{m}_2 \bar{m}_3 \bar{m}_4) d_{\bar{m}_1}^\dagger d_{\bar{m}_2} d_{\bar{m}_3}^\dagger d_{\bar{m}_4} \quad (1)
 \end{aligned}$$

Here, the simplified notation $\bar{m}_x \equiv m_x \sigma_x$ in V_{dd} with $x = 1, 2, 3, 4$ denote the spin-orbital. The E_s represents the onsite energies, where $d_{m\sigma}^\dagger$ ($d_{m\sigma}$) creates (destroys) a hole in the Cu-3d orbital m with on-site energy $\epsilon_d(m)$ and spin σ , while $p_{jn\sigma}^\dagger$ ($p_{jn\sigma}$) creates (destroys) a hole at the O lattice site j , in its 2p orbital n with energy

ϵ_p and spin σ . The Cu-3d orbitals indexed by m are $b_1(d_{x^2-y^2})$, $a_1(d_{3z^2-r^2})$, $b_2(d_{xy})$, $e_x(d_{xz})$, $e_y(d_{yz})$, and the O-2p orbitals indexed by n are p_x, p_y, p_z or a subset of them, as indicated below. All other core levels and the Cu 4s and 4p orbitals are neglected because of their high-energy, which allows for their influence via hybridization to be accounted for by the renormalization of the effective parameters. Finally, the onsite d-hole energies $\epsilon_d(m) = 0$ are assumed to be independent of m , thus omitting the point-charge crystal splitting. This is expected to be a good approximation because it is the hybridization with the O orbitals, included in our model, that accounts for most of the difference between the effective on-site energies of the 3d levels. As a result, the charge-transfer energy $\Delta = \epsilon_p$.

K_{pd} and K_{pp} describe the Cu-O and O-O hoppings, respectively. The labels j, j' run over the positions of the O atoms, $\langle \cdot, j \rangle$ is a sum over the four O adjacent to the j^{th} Cu site, and only NN pp hopping is included. Following Slater and Koster,³³ the Cu-O and O-O hopping integrals T_{mn}^{pd} and $T_{nn'}^{pp}$ are listed in Table I. Throughout the paper, energies are measured in eV.

In the following we focus on four possible models: (i) N3, where $m = b_1$ and $n \in \{p_{x_1}, p_{y_2}\}$, *i.e.* the usual three-band Emery model where only the ligand orbital is kept for each O; (ii) N7, where $m \in \{a_1, b_1, b_2, e_x, e_y\}$ and $n \in \{p_{x_1}, p_{y_2}\}$, *i.e.* multiplet-like physics is added to the Emery model; and (iii) N9, where $m \in \{a_1, b_1, b_2, e_x, e_y\}$ and $n \in \{p_{x_1}, p_{y_1}, p_{x_2}, p_{y_2}\}$, *i.e.* for each O we keep both in-plane 2p orbitals; and (iv) N11, where $m \in \{a_1, b_1, b_2, e_x, e_y\}$ and $n \in \{p_{x_1}, p_{y_1}, p_{z_1}, p_{x_2}, p_{y_2}, p_{z_2}\}$, *i.e.* for each O we keep all three O-2p orbitals.

For the N9 and N11 models we use $T_{b_2}^{pd} = T_{b_1}^{pd}/2$, so that $t_{pd\pi} = \sqrt{3}t_{pd\sigma}/4$. We emphasize that all the Cu-O hybridization parameters $t_{pd}, t_{pp}, t_{pd\sigma}, t_{pd\pi}, t_{pp\sigma}, t_{pp\pi}$ are taken to be positive, and the signs due to the orbitals' overlap (see Fig. 1) are explicitly indicated in Table I.

TABLE I: The Cu-O and O-O hopping integrals T_{mn}^{pd} and $T_{nn'}^{pp}$ with $m \in \{b_1(d_{x^2-y^2}), a_1(d_{3z^2-r^2}), b_2(d_{xy}), e_x(d_{xz}), e_y(d_{yz})\}$ for various models. The hoppings involving $p_{x_3}, p_{y_3}, p_{x_4}, p_{y_4}$ follow the sign convention illustrated in Fig. 1.

m	N3		N7		N9			
	$T_{mx_1}^{pd}$	$T_{my_2}^{pd}$	$T_{mx_1}^{pd}$	$T_{my_2}^{pd}$	$T_{mx_1}^{pd}$	$T_{my_1}^{pd}$	$T_{mx_2}^{pd}$	$T_{my_2}^{pd}$
b_1	$-t_{pd}$	t_{pd}	$-t_{pd}$	t_{pd}	$-\sqrt{3}t_{pd\sigma}/2$	0	0	$\sqrt{3}t_{pd\sigma}/2$
a_1			$t_{pd}/\sqrt{3}$	$t_{pd}/\sqrt{3}$	$-t_{pd\sigma}/2$	0	0	$-t_{pd\sigma}/2$
b_2					0	$t_{pd\pi}$	$t_{pd\pi}$	0

m	N11					
	$T_{mx_1}^{pd}$	$T_{my_1}^{pd}$	$T_{mx_2}^{pd}$	$T_{my_2}^{pd}$	$T_{mx_2}^{pd}$	$T_{my_2}^{pd}$
b_1	$-\sqrt{3}t_{pd\sigma}/2$	0	0	0	$\sqrt{3}t_{pd\sigma}/2$	0
a_1	$-t_{pd\sigma}/2$	0	0	0	$-t_{pd\sigma}/2$	0
b_2	0	$t_{pd\pi}$	0	$t_{pd\pi}$	0	0
e_x	0	0	$t_{pd\pi}$	0	0	0
e_y	0	0	0	0	0	$t_{pd\pi}$

N3/N7		N9/N11			
$T_{x_1y_2}^{pp}$	$2T_{x_1x_2}^{pp}$	$2T_{x_1y_2}^{pp}$	$2T_{x_2y_1}^{pp}$	$2T_{y_1y_2}^{pp}$	
t_{pp}	$t_{pp\pi} - t_{pp\sigma}$	$t_{pp\pi} + t_{pp\sigma}$	$t_{pp\pi} + t_{pp\sigma}$	$t_{pp\pi} - t_{pp\sigma}$	

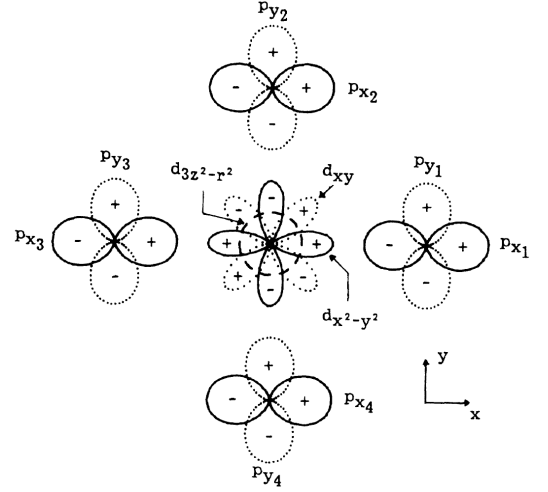


FIG. 1: Schematic view of the orbitals involved in our model calculations, adapted from Eskes's previous related work.¹⁴ The Cu d_{xz}, d_{yz} and the O p_z orbitals are not shown. Note that only the four O that are adjacent to the Cu impurity are depicted, however we consider the full O square lattice.

In this impurity model, the single electron removal eigenstates of the undoped Cu- d^{10} system are due to the hybridization of various Cu- d^9 configurations with the full O band $2p^6$, in other words there is a single hole in the system and the problem can be solved trivially. As expected, if the bottom of the oxygen band at $\Delta - 4t_{pp} > \epsilon_d$, then the system lies in the positive charge-transfer regime, where the lowest energy electron removal state is dominated by an (antibonding) orbital of b_1 symmetry that has predominantly Cu- d^9 character; this is mixed with a ligand hole $d^{10}\bar{L}$ states which have a low amplitude of probability. This confirms that if there is a single hole in the system, it is indeed located primarily on the Cu as in the ground state of the undoped cuprates.

Photoemission or doping of the system with one hole from its ground state of mainly d^9 character removes another electron. The resulting two-hole problem is exactly solvable using the Cini-Sawatzky method³⁴. The two-hole problem requires taking into account the d-d Coulomb and exchange interactions $U(mm'm''m''')$ described by V_{dd} . These are listed in Table II, which contains the interaction matrices for all singlet/triplet irreducible representations of the D_{4h} point group spanned by two d holes, in terms of the Racah parameters A, B , and C . Throughout the paper, the free-ion values $B = 0.15$ eV, $C = 0.58$ eV are adopted and A is treated as a variable.

If we chose to focus on relevance to experiments, we would need to calculate the d -electron removal spectrum $A_d^\Gamma(\omega)$ which can be compared to photoemission experiments, and the d^8 partial density of states (PDOS) for the various two-hole irreducible representations (symmetry channels) $A_{d^8}^\Gamma(\omega)$, linked to the resonant

TABLE II: Irreducible representations spanned by two d holes (d^8) and corresponding Coulomb and exchange matrix elements in terms of Racah parameters A, B, C . The basis functions are based on the single hole irreducible representations: $b_1(d_{x^2-y^2}), a_1(d_{3z^2-r^2}), b_2(d_{xy}), e_x(d_{xz}), e_y(d_{yz})$. Throughout the paper, the free-ion values $B = 0.15$ eV, $C = 0.58$ eV are adopted and A as a variable is also often referred to as Hubbard U , whose value varies in different materials.

${}^1\mathbf{A}_1$	a_1^2	b_1^2	b_2^2	$(e_x^2 + e_y^2)/\sqrt{2}$				
a_1^2	$A + 4B + 3C$	$4B + C$	$4B + C$	$\sqrt{2}(B + C)$				
b_1^2	$4B + C$	$A + 4B + 3C$	C	$\sqrt{2}(3B + C)$				
b_2^2	$4B + C$	C	$A + 4B + 3C$	$\sqrt{2}(3B + C)$				
$(e_x^2 + e_y^2)/\sqrt{2}$	$\sqrt{2}(B + C)$	$\sqrt{2}(3B + C)$	$\sqrt{2}(3B + C)$	$A + 7B + 4C$				
${}^1\mathbf{A}_2$	b_1b_2	${}^3\mathbf{B}_1$	a_1b_1	${}^3\mathbf{B}_2$	a_1b_2			
b_1b_2	$A + 4B + 2C$	a_1b_1	$A - 8B$	a_1b_2	$A - 8B$			
${}^3\mathbf{A}_2$	b_1b_2	e_xe_y	${}^1\mathbf{B}_1$	a_1b_1	$(e_x^2 - e_y^2)/\sqrt{2}$	${}^1\mathbf{B}_2$	a_1b_2	e_xe_y
b_1b_2	$A + 4B$	$6B$	a_1b_1	$A + 2C$	$2\sqrt{3}B$	a_1b_2	$A + 2C$	$2\sqrt{3}B$
e_xe_y	$6B$	$A - 5B$	$(e_x^2 - e_y^2)/\sqrt{2}$	$2\sqrt{3}B$	$A + B + 2C$	e_xe_y	$2\sqrt{3}B$	$A + B + 2C$
${}^1\mathbf{E}$	e_xb_1	e_xa_1	e_yb_2	${}^1\mathbf{E}$	e_yb_1	e_ya_1	e_xb_2	
e_xb_1	$A + B + 2C$	$-\sqrt{3}B$	$-3B$	e_yb_1	$A + B + 2C$	$\sqrt{3}B$	$3B$	
e_xa_1	$-\sqrt{3}B$	$A + 3B + 2C$	$-\sqrt{3}B$	e_ya_1	$\sqrt{3}B$	$A + 3B + 2C$	$-\sqrt{3}B$	
e_yb_2	$-3B$	$-\sqrt{3}B$	$A + B + 2C$	e_xb_2	$3B$	$-\sqrt{3}B$	$A + B + 2C$	
${}^3\mathbf{E}$	e_xb_1	e_xa_1	e_yb_2	${}^3\mathbf{E}$	e_yb_1	e_ya_1	e_xb_2	
e_xb_1	$A - 5B$	$-3\sqrt{3}B$	$3B$	e_yb_1	$A - 5B$	$3\sqrt{3}B$	$-3B$	
e_xa_1	$-3\sqrt{3}B$	$A + B$	$-3\sqrt{3}B$	e_ya_1	$3\sqrt{3}B$	$A + B$	$-3\sqrt{3}B$	
e_yb_2	$3B$	$-3\sqrt{3}B$	$A - 5B$	e_xb_2	$-3B$	$-3\sqrt{3}B$	$A - 5B$	

photoemission.¹⁴ They are defined by

$$\begin{aligned}
 A_d^\Gamma(\omega) &= -\frac{1}{\pi} \sum_{mm'} \lim_{\delta \rightarrow 0} \Im G_{dd}(m, m', \omega + i\delta; \Gamma) \\
 A_{ds}^\Gamma(\omega) &= -\frac{1}{\pi} \sum_{mm'} \lim_{\delta \rightarrow 0} \Im G_{ds}(m, m', \omega + i\delta; \Gamma)
 \end{aligned} \quad (2)$$

with

$$\begin{aligned}
 G_{dd}(m, m', z; \Gamma) &= \langle \psi_{g.s.} | d_{m'} \hat{G}(z) d_m^\dagger | \psi_{g.s.} \rangle \\
 G_{ds}(m, m', z; \Gamma) &= \langle 0 | d_{m'} d_m \hat{G}(z) d_m^\dagger d_{m'}^\dagger | 0 \rangle \\
 \hat{G}(z) &= (z - \hat{H})^{-1}, z = \omega + i\delta
 \end{aligned} \quad (3)$$

Here, $|0\rangle$ is the Cu-3d¹⁰ + O-2p⁶ state, *i.e.* the state with no holes, while $|\psi_{g.s.}\rangle$ is the one-hole ground-state.

For our purposes, however, it suffices to obtain their common part, namely the component of d^8 partial density of states $A^\Gamma(\omega)$ which assumes that one hole has already occupied the b_1 orbital (remember that $d_{b_1}^\dagger |0\rangle$ is the dominant contribution to $|\psi_{g.s.}\rangle$):

$$\begin{aligned}
 A^\Gamma(\omega) &= -\frac{1}{\pi} \sum_m \lim_{\delta \rightarrow 0} \Im G_d(m, b_1, \omega + i\delta; \Gamma) \\
 G_d(m, z; \Gamma) &= \langle 0 | d_{b_1} d_m \hat{G}(z) d_m^\dagger d_{b_1}^\dagger | 0 \rangle
 \end{aligned} \quad (4)$$

We focus primarily on $G_d(m, z; \Gamma)$ from now on, but all other propagators $G_{dd}(m, m', z; \Gamma)$ and $G_{ds}(m, m', z; \Gamma)$ can be calculated similarly.

B. Variational exact diagonalization

We use variational exact diagonalization to calculate the propagator $G_d(m, z; \Gamma)$. The two-hole states in the variational space are of three possible types: (a) both holes are on the Cu; (b) one hole is on the Cu and one on an O; and (c) both holes are on O sites. All states in (a) are included in the variational space. For the (b) and (c) states, we impose a cutoff \mathbf{R}_c between the O hosting the hole(s) and the Cu. Obviously, $\mathbf{R}_c \rightarrow \infty$ recovers the full Hilbert space. We typically set $R_c = 20$ for the results shown below. This suffices for convergence to be reached for all the bound states. Unless we use a very large η , the continua are not yet fully converged for this R_c , instead they look like a collection of peaks whose number increases with R_c . The upper and lower bandedges are already converged, however, and that is all the information relevant for our analysis.

Within this variational space, we set up the Hamiltonian matrix for each irreducible representation and use standard exact diagonalization to calculate the corresponding propagators via Lanczos diagonalization.

III. RESULTS

Before proceeding, we remark that throughout the paper, we adopt the usual convention of photoemission spectroscopies that the electron removal energy, or the

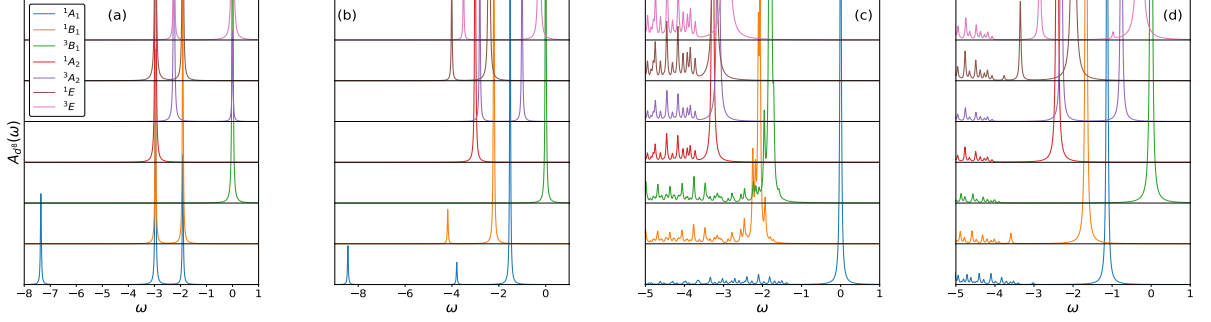


FIG. 2: (Color online) The two-hole spectra $A^\Gamma(\omega)$ calculated for various irreducible representations Γ in the seven-orbital (N7) model in the cases of (a) single Cu- d^8 ion with onsite energies $\epsilon_d(m) = 0$, (b) single Cu- d^8 ion including the additional ligand field splitting³⁵, and single Cu impurity in a lattice of oxygen with finite Cu-O hybridization corresponding to two characteristic cases with differing two-hole ground state of 1A_1 (c) and 3B_1 (d) symmetry respectively. The parameters are (c) $\Delta = 2.75$ eV, $A = 6.5$ eV and (d) $\Delta = 6.5$ eV, $A = 2.5$ eV with $t_{pd} = 1.5$ eV, $t_{pp} = 0.55$ eV. The chemical potential, taken to be zero energy, is chosen as the lowest energy of two-hole state.

hole energy, increases to the left while the energy of the electron addition states increases to the right. The chemical potential, taken to be the zero energy, is chosen at the lowest energy of the two-hole state.

Figure 2 illustrates the two-hole spectra $A^\Gamma(\omega)$ for various irreducible representations Γ in the seven-orbital (N7) model in the cases of (a) single Cu- d^8 ion with onsite energies $\epsilon_d(m) = 0$, (b) single Cu- d^8 ion including the additional ligand field splitting³⁵, and single Cu impurity in a lattice of oxygen with finite Cu-O hybridization corresponding to two characteristic cases with differing two-hole ground states of 1A_1 (c) and 3B_1 (d) symmetry respectively. In the limiting case of $t_{pd} = 0$, the two d holes can have $^1S, ^3P, ^1D, ^3F, ^1G$ configurations, whose energies are listed *e.g.* in Ballhausen.³⁶ As shown in Fig. 2(a), our two-hole spectra $A_{ds}^\Gamma(\omega)$ indeed consist of one or more discrete peaks located at these energies; the number of peaks and their corresponding spectral weights depend on the singlet/triplet nature of the irreducible representation Γ .

Note that the inclusion of the ligand field splittings in Fig. 2(b) only induces modest shifts of the peaks and modification of their spectral weights. In contrary, hybridization with the O band results in a significant spreading of the spectral weights over a much wider energy range, and a complete re-ordering of the low-energy, multiplet-like bound states. Indeed, for this realistic value of $t_{pd} = 1.5$ eV, there is no significant correspondence between the bound peak positions and the multiplets in the atomic limit of $t_{pd} = 0$; neither the splittings between the bound peaks, nor even their order, mimic what is found in the atomic multiplet. Instead, of great importance is that for a not too large Δ (see panel c), the lowest energy state is not the expected triplet according to the Hund's rule but a singlet state; and the first triplet state lies at more than 1.5 eV higher energy. Therefore, our results caution against the approach of

using Wannier functions together with A, B, C Racah parameters renormalized so as to obtain an atomic limit multiplet similar to the one produced by the strong hybridization. Fig. 2 demonstrates that the two have very different splittings and even ordering of the peaks in the various symmetry channels.

From now on we focus on the case where the lowest energy two-hole ground state is of 1A_1 symmetry, as illustrated in Fig. 2(c). There is a clearly visible low-energy discrete peak, proving that for these parameters the two holes form a bound state which is a linear combination of two holes on Cu, one hole on Cu and the other on O, and two holes on O, i.e. the configurations of d^8, d^9L and $d^{10}L^2$. The lowest energy state for adding one hole to a Cu d^9 state as in the hole doped cuprates would be a bound state of 1A_1 symmetry similar to the ZRS as the lowest energy state. According to the Fig. 2, this bound state would be separated from a continuum corresponding to the doped hole in an O-2p band by about 1 eV, which is indeed close to what is observed in ARPES experiments of the cuprates. In addition to the broadening and appearance of bound states beyond the continua, the hybridization also introduces the ligand field like splittings which will mix the various atomic multiplets. Note that for these parameter values, only the 1A_1 peak is clearly below the corresponding continuum, and thus a truly bound state; the other peaks are inside the lower edge of their continua. At even higher energies lies the two hole continuum, where both holes move freely in the O lattice and the Cu is in a d^{10} state; this is superimposed over strong resonances where Cu multiplet lines hybridize with (and are shifted around by) this continuum. All this forms a very broad structure with mixed character and is basically the origin of the so called “waterfall”, a name coined by Lanzara et al³².

Of most interest are three lowest peaks, of which the lowest one, with 1A_1 symmetry, is the first ionization

state starting from Cu- d^9 . Its eigenstate is

$$|\psi\rangle = \sqrt{0.072}|b_1b_1\rangle + \sqrt{0.549}|b_1L_{b_1}\rangle + \sqrt{0.054}|b_1L'_{b_1}\rangle + \sqrt{0.275}|d^{10}L^2\rangle + \dots \quad (5)$$

where \dots represents states having a_1a_1, b_2b_2, ee characters, whose probabilities add up to less than 1%. Here L_{b_1} denotes one hole in a linear combination of O orbitals nearest to the Cu impurity, with overall b_1 symmetry. We emphasize that this weight distribution is almost independent on the number of orbitals considered, whether the N3, N7, N9, or N11 models. This shows that the ground-state is only about 55% ZRS-like, *i.e.* $|b_1L_{b_1}\rangle$. L_{b_1} denotes the configurations where the hole is on the second, third, *etc.* rings of O ions, which strictly speaking are discarded by the ZRS. The strong mixing of the ground state with the $d^{10}L^2$ state is the reason for the strong antiferromagnetic exchange interaction which stabilizes the singlet. It is worth noting that this strong wave function mixing is strongly dependent on t_{pd} , which in turn is strongly dependent on the interatomic distance between Cu and the nearest-neighbor O. This is the origin of a possibly strong electron-phonon and magnon-phonon coupling.

The second and third lowest peaks are the high spin 3B_1 state and the singlet 1B_1 state respectively. All these results are qualitatively similar to those reported in previous work by Eskes *et al.*^{13,14}. The quantitative differences, especially the differences in the weights of various continua, are due to how the O band is modelled (realistic tight-binding model in our work, *vs.* featureless semi-elliptical DOS in theirs).

Next we elaborate on the case where the lowest energy two-hole ground state is of 3B_1 symmetry, as illustrated in Fig. 2(d). To obtain this we adopted $A - \Delta = -4$ eV, which puts the system well into the Mott Hubbard rather than charge transfer gap of the ZSA classification scheme. The major difference from the case shown in Fig. 2(c) is the order of lowest peaks, which changed to be of $^3B_1, ^3E, ^3A_2$ symmetries from those of $^1A_1, ^3B_1, ^1B_1$ symmetries. Furthermore, it is clear that the conventional three-orbital (N3) model cannot capture the lowest bound state any more due to the lack of the involvement of the $a_1(d_{3z^2-r^2})$ orbital.

To investigate the effects of including more Cu-3d and/or O-2p orbitals in the model Hamiltonians, Figure 3 compares the two-hole spectra $A^\Gamma(\omega)$ calculated for the (a,d) seven-orbital (N7), (b,e) nine-orbital (N9), and (c,f) eleven-orbital (N11) models for two characteristic parameter sets corresponding to the low spin (singlet) (a-c) and high spin triplet (d-f) cases. The comparison between N7 and N9/N11 models illustrates the impact of including additional π -bonding oxygen orbitals. The additional hybridization with Cu- $b_2(d_{xy})$ orbital extends the continua to lower energies for all the symmetries, which causes a much smaller difference between the continuum bottom of various A and B types of symmetries. This clearly demonstrates the

importance of having all the continua in place correctly in order to decide which is the lowest energy state. For example, if the 1A_1 continuum would also be involved in the hybridization with the 3B_1 or 1B_1 state, these states would be appreciably closer to the 1A_1 lowest energy state and even cross it. This could happen if we could take into account the full lattice of Cu- d^9 states in the starting configuration, for example, as done in the exact diagonalization study of the large cluster with 32 Cu sites and 64 O sites by Lau *et al.*¹². It is important to note that Lau indeed found a very strong ferromagnetic coupling between the Cu sandwiching an O hole, which indicates that our impurity limit could be different from what happens in the actual crystal although the experiments of cuprates did agree with our classification for the undoped system. Strong hole doping however could strongly modify these conclusions. This also questions the use of single site DMFT or single orbital cluster DMFT results with regard to the relevance for the full problem which includes both O and Cu states explicitly in the cluster.

In the isolated Cu atom, the two-hole ground-state has 3B_1 symmetry (Hund's rule), while, as shown in Fig. 2(c), a strong enough hybridization with the O bands favors a ground-state with 1A_1 symmetry, *i.e.* there is a high spin to low spin transition. To fully characterize the various possible symmetries of the ground-state, in Figure 4 we show phase diagrams in the full parameter space. In panel (a), we plot a $A - \Delta$ *vs.* $2t_{pd}$ phase diagram, which can be directly compared against that shown in Ref. 13. It shows the phase boundaries for obtaining the lowest peak with 1A_1 (blue curve) and with 3B_1 (red curve) symmetries, respectively, for an O bandwidth $W = 4.4$ eV ($t_{pp} = 0.55$ eV). Furthermore, the green curve shows the phase boundary separating the ground state of 1A_1 (low spin) and 3B_1 (high spin) character. The three different types of ground-states are filled by different colors: region I denotes the absence of a bound ground-state state, *i.e.* the doped hole moves freely in the O lattice instead of being bound to the Cu hole. In regions II and III there is a bound ground state with 3B_1 and 1A_1 symmetry, respectively. Clearly, region III is physically relevant to cuprates.

While this phase diagram is qualitatively similar with Eskes's corresponding phase diagram,¹³ there are again quantitative differences between the two. There is a shift of the critical value of the pd hybridization needed to obtain a bound state with 1A_1 symmetry from their value $T(B_{1g}) = 2t_{pd} \approx 1.6$ eV to our value of ≈ 1.0 eV. In addition, the lines separating the various regions have quite different slopes. These non-trivial quantitative differences are due to the difference in how the O bath is modeled. One of the main reasons for this difference is that in the Eskes approach the ligand hole states are all spread equally over the hemispherical band while in our tight-binding band structure the b_1 symmetry hole states are concentrated at the bottom of the hole density of states making the appearance of a two-hole 1A_1 bound

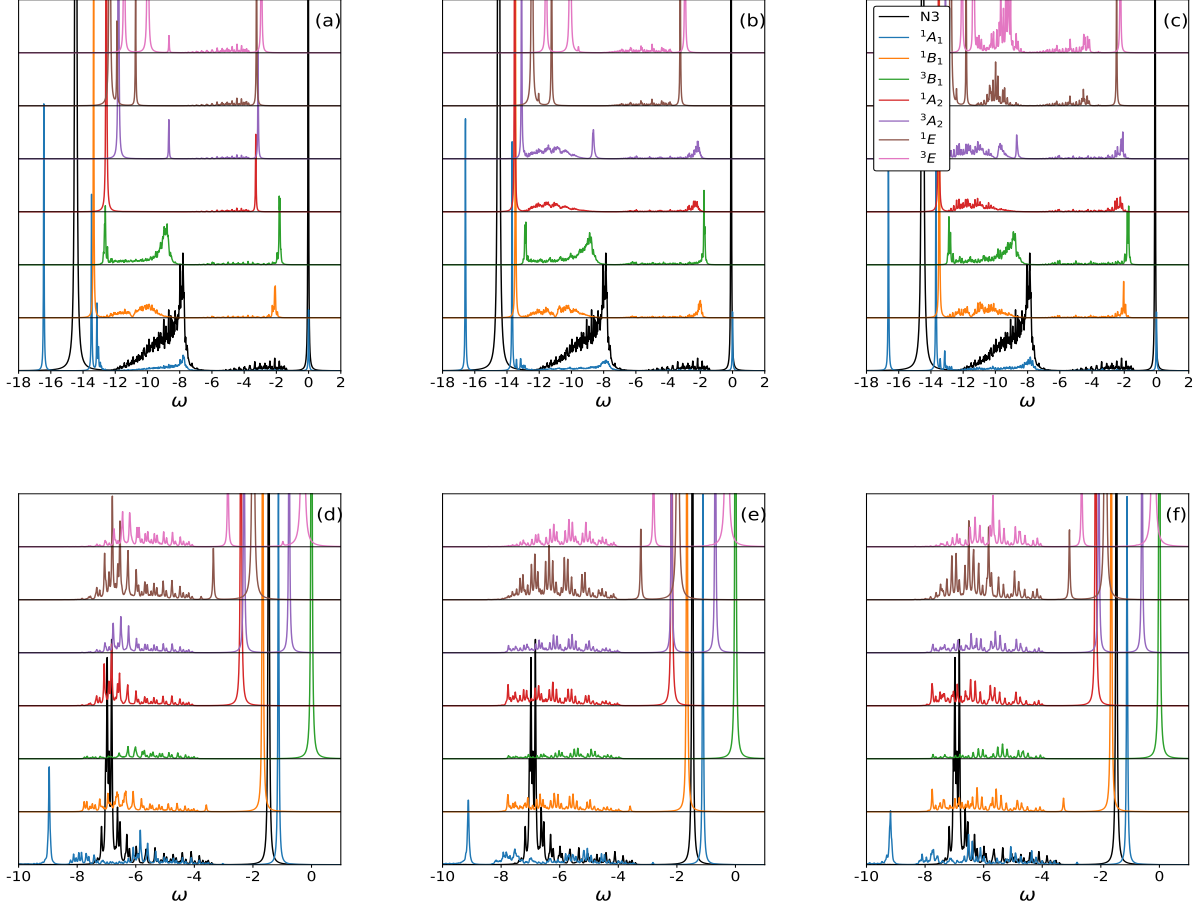


FIG. 3: (Color online) The comparison of two-hole spectra $A^\Gamma(\omega)$ calculated for various irreducible representations Γ in the (a,d) seven-orbital (N7), (b,e) nine-orbital (N9), and (c,f) eleven-orbital (N11) models for two characteristic parameter sets corresponding to the low spin (singlet) (a-c) and high spin triplet (d-f) cases. The spectra of N3 model (black curve) is plotted for comparison as well. The parameters are (a-c) $\Delta = 2.75$ eV, $A = 6.5$ eV and (d-f) $\Delta = 6.5$ eV, $A = 2.5$ eV with (a, d) $t_{pd} = 1.5$ eV, $t_{pp} = 0.55$ eV and (b-c, e-f) $t_{pd\sigma} = \sqrt{3}$ eV, $t_{pd\pi} = 0.75$ eV, $t_{pp\sigma} = 0.9$ eV, $t_{pp\pi} = 0.2$ eV. For the N3 model, we use $U_{dd} = A + 4B + 3C$, $t_{pp} = 0.55$ eV.

state possible at even lower t_{pd} . Another important difference caused by the same effect is that in our case the splitting between the 1A_1 and the 3B_1 peaks is larger than that in the Eskes picture (it is even larger for the 1B_1 case). This results in a stabilization of the 1A_1 state to even more negative $A - \Delta$ or extending even further into the Mott Hubbard regime of the ZSA classification scheme.

Figure 4(b) illustrates the impact on the phase boundaries of the number of O-2p orbitals kept in the model: full/dashed lines are for the N7/N9 model. The conventional relations $t_{pd} \approx \sqrt{3}t_{pd\sigma}/2 = 2t_{pd\pi}$ and $t_{pp\sigma} = 0.9$ eV, $t_{pp\pi} = 0.2$ eV are used for the N9 model. Clearly, adding the second in-plane O-2p orbital in the model does not have significant effects on the phase boundaries, except to slightly shift the I-III boundary. The same is true if the p_z orbitals are also included, in

N11 (not shown). For comparison, the black line denotes the critical $A - \Delta$ for the appearance of low-energy bound state of Zhang-Rice singlet nature in the N3 model. At larger t_{pd} this agrees well with the 1A_1 boundary for N7 model, suggesting minor differences there between the N3 and N7 models.

Two-dimensional phase diagrams like those of Figure 4 may be expected to change depending on whether the $A - \Delta$ axis is spanned by changing A while keeping Δ constant, or by changing Δ while keeping A constant, or by some other protocol. In Fig. 5 we show how the phase diagram evolves with the charge transfer energy Δ . The rather weak dependence of the $A - \Delta$ vs. t_{pd} phase boundaries upon Δ confirms the importance of the energy separation between A and Δ . Specifically, as Δ governs the energy difference between the d^9 and $d^{10}L$ state, $A - \Delta$ governs the average energy difference

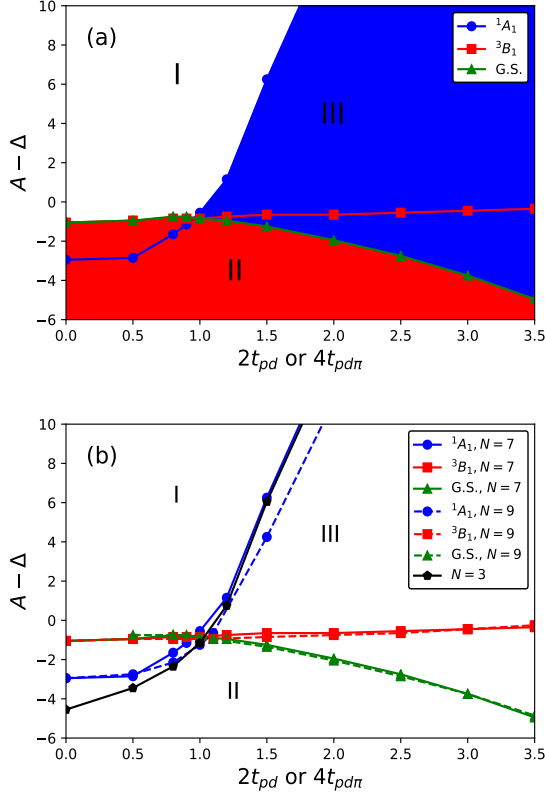


FIG. 4: (Color online) (a) N7 one-doped hole phase diagram for $\Delta = 2.75$ eV and oxygen bandwidth $W = 4.4$ eV, *i.e.* $t_{pp} = 0.55$ eV. Region I has no bound state, while in regions II and III and the doped hole is bound to the Cu hole in a complex with 3B_1 and 1A_1 symmetry, respectively. (b) Comparison between N3, N7 and N9 phase diagrams. The conventional relations $t_{pd} \approx \sqrt{3}t_{pd\sigma}/2 = 2t_{pd\pi}$ and $t_{pp\sigma} = 0.9$ eV, $t_{pp\pi} = 0.2$ eV are adopted in the N9 model. For the N3 model, we use $U_{dd} = A + 4B + 3C$, $t_{pp} = 0.55$ eV. The black line denotes the boundary for the appearance of the ZRS like states in the N3 model. The colored lines indicate the phase boundaries for obtaining a sharp “bound like state” at low energy with 1A_1 (blue curve) and 3B_1 (red curve) symmetries.

between d^8 and d^9L . If A is less than Δ , we are closer to a Mott-Hubbard limit than a charge-transfer gap limit. In that case, the d^8 triplet is the lowest energy electron removal state as clearly seen in Fig. 4 although the singlet lowest energy state extends well into this negative $A - \Delta$ region.

To further characterize the evolution of the ground state from region II (3B_1) to III (1A_1), Fig. 6 plots how the weights of the dominant components to the ground state change with A , for realistic values of $t_{pd} = 1.3$ eV, $\Delta = 3.5$ eV. As expected (see also Eq. 5), in region III the ground state is dominated by the $b_1L_{b_1}$ singlet, which is the equivalent of the ZRS. In region II, the high spin ground state is dominated by the a_1b_1 triplet. However, in both cases there are significant contributions from other configurations with

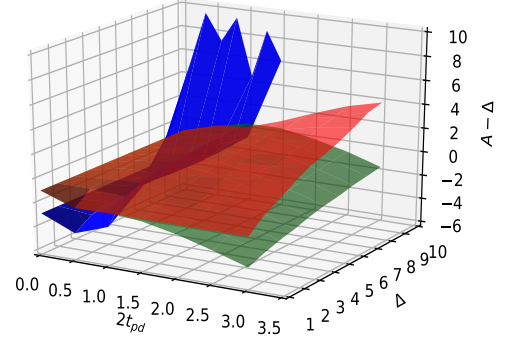


FIG. 5: (Color online) Weak dependence of the phase boundaries of N7 phase diagram showed in Figure 4(a) (with the same color conventions) on the charge transfer energy Δ .

the correct symmetry. This shows that overly simplistic models, which project out everything but the largest probability component, may be qualitatively correct but will certainly not be quantitatively accurate for realistic values of the parameters.

Finally, we compare the results of the conventional three-orbital Emery model (N3 in our notation) against the N7 and N9 results, to see if the multiplet physics plays any essential role at values of the parameters believed to be reasonable for cuprates. To achieve this, we performed the N3 calculation with the same Cu-O hybridization, O-2p hopping integrals, and charge transfer energy Δ in region III of the phase diagram as in the N7 model, but keeping only the $b_1(d_{x^2-y^2})$ orbital with a Hubbard-like $U_{dd} = A + 4B + 3C$ (see Table I).

Figure 7(a) compares the spectral weight with 1A_1 symmetry for the three models. Clearly, the ground-state peak and the intermediate energy continua due to Cu-O hybridization are in good agreement. However, the high energy regions ($\omega \approx 10.0$ eV) of the N7 and N9 models

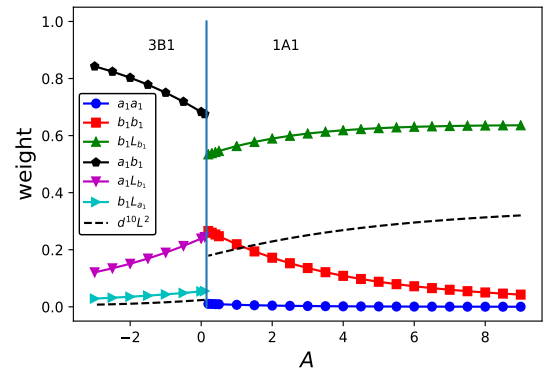


FIG. 6: (Color online) Variation of the ground state weights of the dominant components versus A , for fixed $t_{pd} = 1.3$ eV, $\Delta = 3.5$ eV. The vertical line denotes the critical value $A = 0.1$ eV separating the two phases.

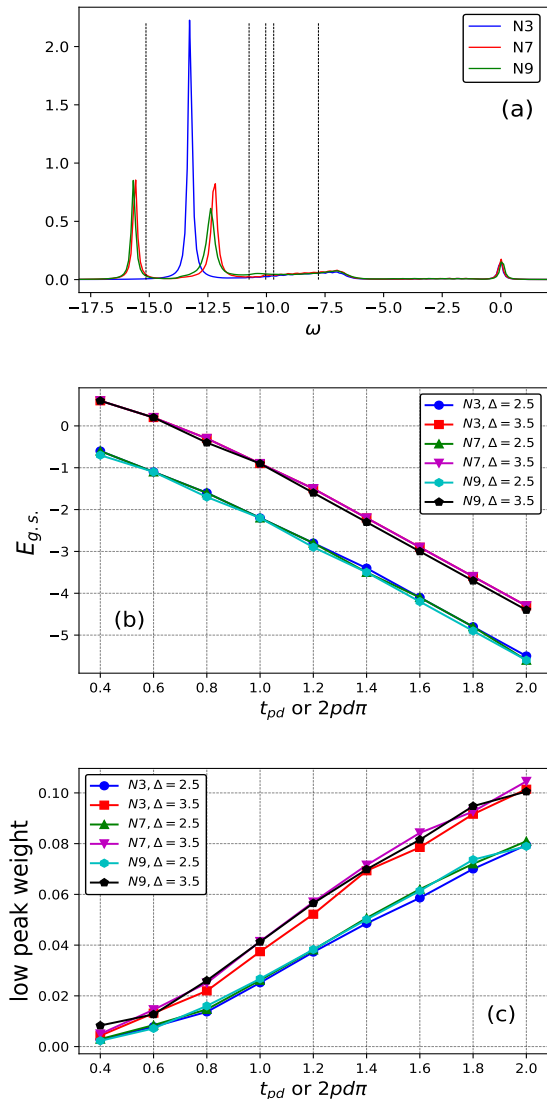


FIG. 7: (Color online) (a) Comparison of two-hole spectra for the N3, N7 and N9 models. Parameters are $\Delta = 3.0$ eV, $A = 6.5$ eV, $U_{dd} = A + 4B + 3C = 8.84$ and $t_{pd} = 1.3$ eV, $t_{pp} = 0.65$ eV, $t_{pd\sigma} = 2.6/\sqrt{3}$ eV, $pd\pi = 0.65$ eV, $t_{pp\sigma} = 1.0$ eV, $t_{pp\pi} = 0.3$ eV; (b-c) the ground-state energy and the weight of its corresponding peak as functions of the Cu-O hybridization t_{pd} and charge-transfer energy Δ .

differ from that of the N3 model, as the latter has a double-occupancy peak at about U_{dd} instead of the full multiplet spectrum of the former.

Figures 7(b) and (c) focus on the ground-state energy and peak weight, respectively. We see that the models are in very good agreement, suggesting that the multiplet physics and/or inclusion of non-ligand O-2p orbitals has little relevance for the nature of the ground-state. These results appear to confirm the validity of the conventional three-orbital Emery model for describing the low energy physics of the cuprates.

As a final note, we remark again about the potential importance of including more than one Cu atoms in addition to explicitly including the O states, as done in Lau's previous calculations¹². This might lead to very different conclusions especially when considering the effects of doping to a level where the ZR like states strongly overlap, which already occurs at less than 10% doping.

IV. CONCLUSION

In summary, we used variational exact diagonalization to revisit the problem of the spectra of two holes doped into an otherwise full CuO_2 layer, modelled as a Cu-d^{10} impurity properly embedded into a square lattice of O-2p⁶. While the relevance of the full Cu multiplet structure was considered before, with results in qualitative agreement with ours, the novelty here is that we use a realistic tight binding band structure for the O band and consider the implications of adding non-ligand 2p orbitals, as well.

We find that using a realistic O-2p band structure does not change qualitatively the two-hole spectra in the various symmetry channels, when compared against those obtained using a featureless, semielliptic band structure. However, there are significant quantitative changes. For example, the region in the phase diagram favoring a bound ground-state with 1A_1 symmetry is enlarged significantly and extends well into the Mott Hubbard region of the ZSA classification scheme. This proves that using a realistic band-structure has non-trivial quantitative consequences, that are important if detailed modelling and comparison to experiments is desired. This is an important lesson for any impurity-type calculations, including for the use of the dynamical mean-field theory (DMFT) approximations. In particular, it is important to include the O-2p states explicitly in the impurity Hamiltonian together with the full multiplet structure, rather than restricting to coupling to a bath of Cu or effective Cu 3d states.

Speaking of approximations, our results also caution against the approach of using Wannier functions together with A, B, C Racah parameters renormalized so as to obtain an atomic limit multiplet similar to the one produced by the strong hybridization. As discussed when analyzing the results from Fig. 2(a), the two have very different splittings and even ordering of the peaks in the various symmetry channels. For example, in order to get the singlet-triplet crossing within an atomic multiplet approach, one would need to have a Hund's rule $J_d < 0$, which is not reasonable. In the original papers describing the effective screening of U , the lack of screening of J_h and other Hund's rule interactions were obtained with the assumption that the covalency and transition metal to oxygen hybridization would be explicitly included in the model Hamiltonians. This is very different from trying to account for the effects of hybridization through

the use of Wannier functions.

Furthermore, we find that the three-orbital Emery model reproduces well the low-energy results obtained in the 1A_1 symmetry channel of the N7 and N9 models. In particular, its ground-state is consistent with the ZRS, but the overlap with the ZRS wavefunction is only around 50% for reasonable values of the parameters. This raises questions about the accuracy of projecting the Emery model onto ZRS, to obtain simple one-band Hamiltonians¹⁷. We point out again the importance of including all the multiplets when discussing energy scales larger than about 1eV as in many of the optical and photoemission spectroscopies. An obvious example is the appearance of the so called “waterfall” feature³² at energies of about 1eV above the lowest energy electron removal state. This can trivially be explained by taking into account all the multiplets and their hybridization with the oxygen bands, forming a broad region in energy where a huge number of bands cross and overlap so that a broad continuum sets in a momentum distribution plot of ARPES spectroscopy.

We also find that adding more O-2p orbitals (in the N9 and N11 models) has essentially no consequences on the 1A_1 symmetry low-energy spectra. All these results seem to confirm the validity of the conventional three-orbital Emery model for describing the low energy physics. However, more care is needed before drawing that conclusion, as the Emery model completely misses the low-energy peaks of other symmetries that are revealed by the full calculation, and which may be relevant to various properties of the cuprates. In fact, it is worth emphasizing that the projection onto different irreducible representations is only possible because we treat a single

Cu impurity, as opposed to a lattice of Cu sites. For a lattice, these various symmetries will mix everywhere in the Brillouin zone except at high-symmetry points, and thus it is questionable whether these states with other symmetries are truly irrelevant. In fact, the study by Lau¹² clearly demonstrates a strong ferromagnetic ordering of the two Cu spins sandwiching an oxygen hole. This is a strong indication that more extended cluster models need to be studied to check whether the influence of the magnetic order and of the hole or electron doping on the stability of the ZRS in single-band Hubbard model scenario, is indeed valid in the doping region where superconductivity arises.

The lower symmetry of the lattice (as opposed to an impurity) may also explain how the z -axis polarization, discussed in the introduction, may be accounted for. The $d_{3z^2-r^2}$, d_{xz} and d_{yz} orbitals have very little contribution to the 1A_1 ground-state, but they contribute significantly to the low-energy peaks in the other symmetry channels. A lattice calculation that breaks the D_{4h} point group symmetry may boost not only their contribution to the ground-state, but also the importance of the O-2p $_z$ orbitals that mostly hybridize with them.

To settle these questions, calculations for the lattice equivalent of the N7 model are needed. Needless to say, an exact solution is a very hard challenge. Instead, it may be possible to obtain accurate results using variational approximations similar to those used here, but extended to a full Cu lattice. We will investigate this next.

Acknowledgements: This work was funded by Stewart Blusson Quantum Matter Institute, Natural Sciences and Engineering Research Council (NSERC) for Canada, and Canada First Research Excellence Fund (CFREF).

-
- ¹ P.W. Anderson, Science **235**, 1196 (1987); G. Baskaran, Z. Zou, and P.W. Anderson, Solid State Commun. **63**, 973 (1987).
 - ² J. Zaanen, G.A. Sawatzky, and J.W. Allen, Phys. Rev. Lett. **55**, 418 (1985).
 - ³ V.J. Emery, Phys. Rev. Lett. **58**, 2794 (1987).
 - ⁴ F. C. Zhang and T. M. Rice, Phys. Rev. B **37**, 3759 (1988).
 - ⁵ A. A. Aligia, M. E. Simon, and C. D. Batista Phys. Rev. B **49**, 13061 (1994).
 - ⁶ F. Lema and A. A. Aligia Phys. Rev. B **55**, 14092 (1997).
 - ⁷ I. Santoso, W. Ku, T. Shirakawa, G. Neuber, X. Yin, M. Enoki, M. Fujita, R. Liang, T. Venkatesan, G.A. Sawatzky, A. Kotlov, S. Yunoki, M. Rubhausen, and A. Rusydi, Phys. Rev. B **95**, 165108 (2017).
 - ⁸ C.P.J. Adolphs, S. Moser, G.A. Sawatzky, and M. Berciu, Phys. Rev. Lett. **116**, 087002 (2016).
 - ⁹ L. H. Tjeng, C. T. Chen, J. Ghijsen, P. Rudolf, and F. Sette, Phys. Rev. Lett. **67**, 501 (1991).
 - ¹⁰ L. H. Tjeng, B. Sinkovic, N. B. Brookes, J. B. Goedkoop, R. Hesper, E. Pellegrin, F. M. F. de Groot, S. Altieri, S. L. Hulbert, E. Shekel, and G. A. Sawatzky, Phys. Rev. Lett. **78**, 1126 (1997).
 - ¹¹ N. B. Brookes, G. Ghiringhelli, O. Tjernberg, L. H. Tjeng, T. Mizokawa, T. W. Li, and A. A. Menovsky, Phys. Rev. Lett. **87**, 237003 (2001).
 - ¹² B. Lau, M. Berciu, and G.A. Sawatzky, Phys. Rev. Lett. **106**, 036401 (2011).
 - ¹³ H. Eskes and G.A. Sawatzky, Phys. Rev. Lett. **61**, 1415 (1988).
 - ¹⁴ H. Eskes, L.H. Tjeng, and G.A. Sawatzky, Phys. Rev. B **41**, 288 (1990).
 - ¹⁵ J. Zaanen and G.A. Sawatzky, Can. J. Phys. **65**, 1262 (1987).
 - ¹⁶ H. Ebrahimnejad, G.A. Sawatzky, and M. Berciu, Nat. Phys. **10**, 951 (2014).
 - ¹⁷ H. Ebrahimnejad, G. A. Sawatzky and M. Berciu, J. Phys.: Cond. Mat. **28**, 105603 (2016).
 - ¹⁸ F. M. F. de Groot, J. C. Fuggle, B. T. Thole, and G. A. Sawatzky, Phys. Rev. B **42**, 5459 (1990).
 - ¹⁹ L. F. Feiner, M. Grilli, and C. Di Castro, Phys. Rev. B **45**, 10647 (1992).
 - ²⁰ A. Bianconi, P. Castrucci, A. Fabrizi, M. Pompa, A. M. Flank, P. Lagarde, H. Katayama-Yoshida, and G. Caletani, Physica C 162-164, 209 (1989); in Earlier and Recent Aspects of Superconductivity, edited by J. G. Bednorz and K. A. Muller, Springer Series in Solid State

- Sciences Vol. 90 (Springer-Verlag, Berlin, 1990), p. 407.
- ²¹ A Bianconi, in Proceedings of the International Conference on Superconductivity-ICSC, Bangalore, 1990, edited by S. K. Joshi, C. N. R. Rao, and S. V. Subramanyam (World Scientific, Singapore, 1990), p. 448.
 - ²² H. Romberg, N. Nucker, M. Alexander, J. Fink, D. Hahn, T. Zetterer, H. H. Otto, and K. F. Renk, Phys. Rev. B **41**, 2609 (1990).
 - ²³ N. Nucker, H. Romberg, X. X. Xi, J. Fink, B. Gegenheimer, and Z. X. Zhao, Phys. Rev. B **39**, 6619 (1989).
 - ²⁴ W. Weber, Z. Phys. B **70**, 323 (1988).
 - ²⁵ D. L. Cox, M. Jarrell, C. Jayaprakash, H. R. Krishnamurthy, and J. Deisz, Phys. Rev. Lett. **62**, 2188 (1989).
 - ²⁶ M. Grilli, C. Castellani, and C. Di Castro, Phys. Rev. B **42**, 6233 (1990).
 - ²⁷ O. Tjernberg, L. H. Tjeng, P. G. Steeneken, G. Ghiringhelli, A. A. Nugroho, A. A. Menovsky, and N. B. Brookes, Phys. Rev. B **67**, 100501(R), (2003).
 - ²⁸ H. Sakakibara, H. Usui, K. Kuroki, R. Arita, and H. Aoki, Phys. Rev. B **85**, 064501 (2012).
 - ²⁹ C.E. Matt et al. Nat. Commun., **9**, 972 (2018).
 - ³⁰ W.M. Li, L. P. Cao, J. F. Zhao, R. Z. Yu, J. Zhang, Y. Liu, Q. Q. Liu, G. Q. Zhao, X. C. Wang, Z. Hu, Q. Z. Huang, H. Wu, H. J. Lin, C. T. Chen, J. S. Kim, G. Stewart, Z. Li, Y. W. Long, Z. Z. Gong, Z. Guguchia, Y. J. Uemura, S. Uchida, C. Q. Jin, arXiv:1808.09425 (2018).
 - ³¹ G. A. Sawatzky and A. Lenselink, Phys. Rev. B **21**, 1790, (1980).
 - ³² J. Graf, G.-H. Gweon, and A. Lanzara, Physica C, **460-462**, 194-197 (2007).
 - ³³ J.C. Slater and G.F. Koster, Phys. Rev. **94**, 1498 (1954).
 - ³⁴ M. Cini, Solid State Commun. **24**, 681 (1977); G. A. Sawatzky, Phys. Rev. Lett. **39**, 504 (1977).
 - ³⁵ We adopt the values in Figure 2 of Ref.¹⁴ for the ligand field splittings. Note that the precise values do not modify the implication in the text.
 - ³⁶ C.J. Ballhausen, Introduction to ligand field theory, McGraw-Hill series in advanced chemistry (1962).